Design optimization of filament wound cylinder by considering process induced residual stresses

PALMIERI Barbara[1,2,a*], BIANCHI Iacopo[3,b], DE PRISCO Nello[2,c], FORCELLESE Archimede[3,d], MANCIA Tommaso[3,e], SIMONCINI Michela[3,f], DE TOMMASO Giuseppe[2,g], PETRICCIONE A.[2,h] and MARTONE Alfonso[1,i]

[1]CNR-IPCB Institute for Polymers and Composites, P.le E Fermi, 80055 Portici (NA) - Italy

[2]Advanced Tools and Moulds, S.r.l., Stab. 13 Z.i. Aversa Nord, Gricignao di Aversa (CE) - Italy

[3]Università Politecnica delle Marche, Via Brecce Bianche 12, 60123 Ancona, Italy

[a]barbara.palmieri@ipcb.cnr.it, [b]i.bianchi@pm.univpm.it, [c]nellodeprisco@atmsrl.com, [d]a.forcellese@pm.univpm.it, [e]t.mancia@pm.univpm.it, [f]m.simoncini@pm.univpm.it, [h]angelo.petriccione@atmsrl.com, [i]alfonso.martone@cnr.it

Keywords: Cure Kinetics, Multi-Physics, CFRP, Viscoelastic

Abstract. The manufacturing process has a significant influence on the product quality of filament wound composite parts. During the filament winding process, a large tensile load to the fibre was applied and maintained during resin curing, resulting in residual stress. This residual stress gradually relaxes due to the fibres' slippage, the matrix's crosslinking, and different coefficients of thermal expansion between composite parts and mandrels. As a result, increasing the number of layers becomes more problematic. In this work, a multiphysics analysis has been carried out to study the effect of the viscoelastic behaviour of the material on the rise of residual stress on thick cylinders. The multiphysics model was developed in COMSOL to predict the temperature distribution and the degree of polymerization during the consolidation process. The optimal cure profile was identified as a function of process parameters to minimize the thermal gradient within the composite element.

Introduction

Thanks to their high stiffness-to-weight ratios, corrosion resistance, and excellent design flexibility, filament wound cylindrical composite parts find extensive applications in the aerospace industry, offshore pipes, underwater vehicles, and high-pressure gas storage [1–4]. For this class of components, the manufacturing process would induce the rise of residual stresses, especially in case of the autoclave curing cycle, unavoidable residual stresses have been extensively documented as a potential hazard to composite structures [5–7]. Upon demoulding, part of these residual stresses is released, resulting in process-induced distortions. This can affect the dimensional accuracy of the composite part, and cause assembly issues, that could even result in the rejection of parts. In some applications the presence of an initial stress state can contribute to relief the working loads, therefore a tension state is applied during the winding process to induce a controlled prestress state. This prestress gradually relaxes as effect of chemical relaxation due to resin curing, and thermal relaxation depending on the temperature profile experienced during the process itself.

For thick composite cylindrical structures, decoupling these factors aids in understanding the quantitative relationship between prestress and residual stress. In fact, the exothermic reaction of resin during the cross-linking process and the low thermal conductivity of material usually lead to an overshoot temperature peak and nonuniform distribution of temperature for thick laminate, resulting in residual stress, possible degradation of the composite and matrix cracks [8,9]. Generally, the manufacturer's recommended cure cycle may not be applicable for thick laminates,

therefore knowing the effect of the cure cycle on residual stress is necessary to reduce residual stresses and increase the mechanical performance of composite parts. Several studies have been conducted to predict the residual stresses in composite by numerical model, but many of these only focus on the material properties in the glassy state [7,10–12].

In this paper, the cure kinetic properties of an epoxy TowPreg have been included in a multiphysics analysis for predicting residual stress. The proposed methodology involves two step analysis, the resin reaction during the cure including the exothermic heat generation and the thermomechanical behaviour when the resin is fully cured. An optimal cure profile has been finally identified by introducing two different dwells to retain the temperature overshoot below the degradation and to avoid temperature/degree of cure mismatches within the domain.

Heat Transfer and Exothermic Cure Modelling

A thermal model was developed to study the time variation of temperature and the degree of cure (DoC) of the thermosetting resin used to impregnate the carbon tow. The Equation governing heat transfer in the resin during the manufacturing process is [13]:

$$\rho Cp \frac{\partial T}{\partial t} = \frac{1}{r}\frac{\partial}{\partial r}\left(k_r \frac{\partial T}{\partial r}\right) + \frac{\partial}{\partial z}\left(k_z \frac{\partial T}{\partial z}\right) + \rho \Delta H_{tot} \frac{\partial \alpha}{\partial t}(1 - V_f) \tag{1}$$

Where T is the temperature, t is the time, ρ and Cp, are the composite material's density and specific heat; k_r and k_z are the thermal conductivity in r and z direction, respectively. The third term of the equation (1) refers to the internal volumetric heat generation linked to the polymerization of the resin. ΔH_{tot} and V_f indicates the total reaction enthalpy and the fibre volume fraction, while $\partial \alpha /\partial t$ is the polymerization's rate, which depends on the DoC (degree of Cure) and temperature (Eq.(2), Kamal and Sourour equation [14]. To resolve the time derivative of the DoC, an ordinary differential equation (ODEs) and differential algebraical equations (DAEs) nodes have been added to the heat transfer one.

$$\frac{\partial \alpha}{\partial t} = k_1 * (1 - \alpha)^n + k_2 * \alpha^m * (1 - \alpha)^n \tag{2}$$

Where n and m are the reaction orders of the four parameters model, while k_1 and k_2 are the rate constants defined by the Arrhenius expression:

$$k_1(T) = A_1 e^{-\frac{E_1}{RT}} ; k_2(T) = A_2 e^{-\frac{E_2}{RT}} \tag{3}$$

Table 1. Kinetic Parameters estimated for the epoxy system considered.

Parameter	Value	Unit
A_1	1.9e3	1/s
A_2	1.5	1/s
E_1	4.34e4	J/mol
E_2	7.5e5	J/mol
n	1.42	
m	1.2	
ΔH_{tot}	350	kJ/kg
R	8.314	J/(mol·K)

E is the activation energy, R is the gas constant (8.314 J/mol K), T is the absolute temperature (K), and A is the pre-exponential factor. The parameters m, n, A_1, A_2, E_1, E_2 have been identified experimentally through Differential Scanning Calorimetry (DSC) tests on the material and reported in Table 1.

In the ODE node, the resin kinetics (Eq.(2)) is represented by the equation (4):

$$f = e_a \frac{\partial^2 \alpha}{\partial t^2} + d_a \frac{\partial \alpha}{\partial t} \qquad (4)$$

Where d_a is the damping term and is unity, while e_a is the mass coefficient and is zero, indicating that the material is modelled starting from the uncured state.

A 2D finite element model of the TowPreg polymerisation process for the autoclave cure cycle has been developed by the Comsol Multiphysics software. The following assumptions were considered in the model, both for the workpiece and the mandrel: (i) the density, the specific heat and the thermal conductivity were assumed constant; (ii) the material was set homogenous and transversely isotropic, and (iii) the heat transfer between the workpiece and the mandrel was taken into account.

The CFRP and mandrel properties used in the FE model are listed in Table 2. The density of the CFRP and the thermal capacity were obtained from data reported in the literature [15,16], while the thermal conductivity was obtained by the mixture rule:

$$\frac{1}{k_c} = \frac{V_f}{k_f} + \frac{V_m}{k_m} \qquad (5)$$

$$k_c = k_f V_f + k_m V_m \qquad (6)$$

Where k_C, k_f and k_m indicate, respectively, the composite's, fibres, and matrix thermal conductivity.

Table 2. Thermal properties of the CFRP component and aluminium mandrel used in the thermomechanical simulation.

Material	Parameter	Value	Unit	Description
Aluminum	ρ_{Al}	2700	kg/m^3	Density
	C_{pAl}	900	J/(kg·K)	Specific Heat
	$k_{r,Al} = k_{z,Al}$	1.2e-5	W/(m·K)	Thermal conductivity
	E_{Al}	69	GPa	Young modulus
	v_{Al}	0.3	-	Poisson modulus
CFRP	ρ_C	1820	kg/m^3	Density
	C_{pC}	1200	J/(kg·K)	Specific Heat
	$k_{r,C}$	1	W/(m·K)	Thermal conductivity
	$k_{z,C}$	200	W/(m·K)	Thermal conductivity
	$E_{r,C}$	8	GPa	Young modulus, radial axis
	$E_{z,C}$	94	GPa	Young modulus, z axis
	v_C	0.3	-	Poisson modulus

Figure 1 shows the surfaces where thermal boundary conditions have been applied in the model. All the external surfaces of the mould and the part were exposed to the autoclave flux and temperature with an initial condition of T_{room} at 20°C. The convective coefficient within the autoclave was set up according to the literature available data [17,18]. The mandrel is plugged by the rack holder therefore the air inside could be considered in no flow condition.

Autoclave flow

$h_\infty \ 100 \ W/(K \ m^2) \ T_\infty = Autoclave \ temperature$

CFRP part

mandrel

no flow condition inside the mandrel

$h_\infty \ 5 \ W/(K \ m^2)$
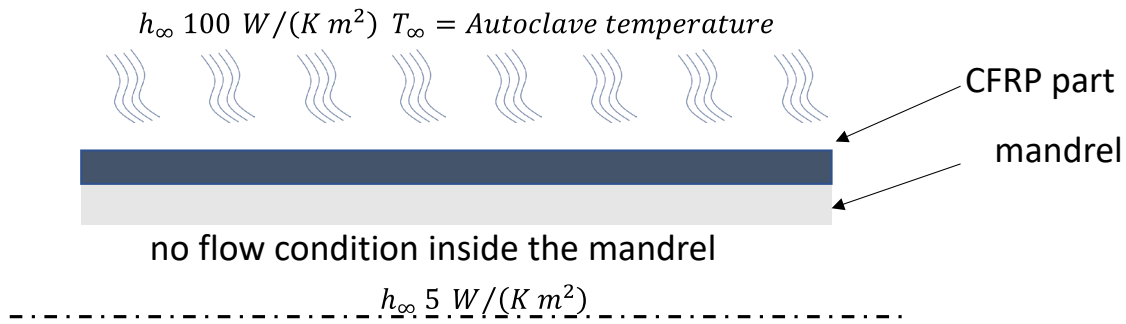
Figure 1. Boundary Conditions for the Thermal Analysis.

In order to take into account, the heating generated by the polymerisation process, an additional heat source has been considered for the composite part. Two different temperature profiles were investigated to optimize the curing cycle to minimize the residual stress occurring in the workpiece. The first one, shown in Figure 2a, consists of a heating ramp from T_{room} to 120°C at 1.5°C min and a dwell time of 120 minutes, and then a cooling ramp of 2°C/min. The optimized curing cycle consists of an initial temperature of 20 °C and DoC of 0.0001. Then the temperature increases to 90°C with a temperature raising rate of 1.5°C/min. Then, a first holding stage of 120 min is applied.

After the dwell, the part is heated at 1.5 °C/min to 120°C to the second holding stage. After that, the laminate is heated at 120°C for 60 min. At last, the temperature drops to 20°C at 2 C°/min. Figure 2 shows the thermal cycle considered.

a)

b)
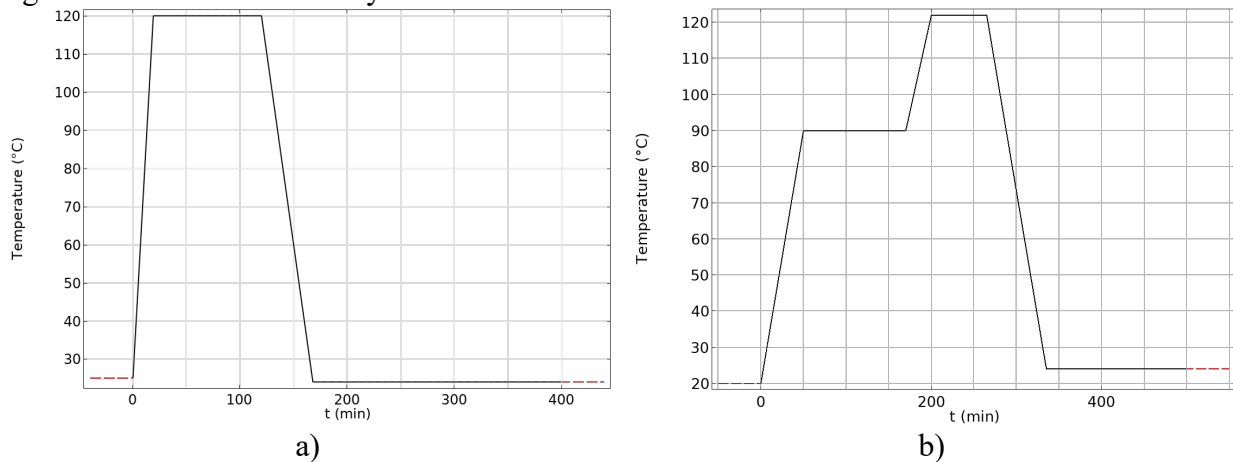
Figure 2. a) Standard thermal cure cycle; b) Optimized thermal cure cycle

Coupled Heat Transfer and Mechanical Analysis

Thermo-mechanical properties of composite material are influenced by the interaction between fibres and matrix. In the present analysis, the thermo-mechanical properties have been characterized by experimental tests on the composite ply. Constitutive equation was therefore written at macro-level homogenized scale. To calculate the temporal evolution of the stress, the mechanical equilibrium equations have been imposed on the whole laminate,

$$\nabla \cdot S + b = 0 \tag{7}$$

Where **b** is the body force vector, neglected in the present analysis. In cylindrical coordinates, the mechanical equilibrium equations, considering also the axial symmetric conditions, are given by:

$$\frac{\partial \sigma_r}{\partial r} + \frac{\partial \tau_{rz}}{\partial z} + \frac{\sigma_r - \sigma_\theta}{r} = 0 \tag{8}$$

$$\frac{\partial \tau_{r\theta}}{\partial r} + \frac{\partial \tau_{\theta z}}{\partial z} + 2\frac{\tau_{r\theta}}{r} = 0 \tag{9}$$

$$\frac{\partial \tau_{rz}}{\partial r} + \frac{\partial \sigma_z}{\partial z} + \frac{\tau_{rz}}{r} = 0 \tag{10}$$

Boundary conditions require radial stress to be the opposite of autoclave chamber environmental pressure $p(t)$ and absence of tangential stress on the external laminate surface:

$$\sigma_r(R_{ext}^e, t) = -p(t), \qquad \tau_{r\theta}(R_{ext}^e, t) = 0, \qquad \tau_{rz}(R_{ext}^e, t) = 0 \tag{11}$$

Where R_{ext}^e is the external radius of the composite part. A scheme of the mechanical boundary conditions imposed is reported in Figure 3.

These boundary conditions are then coupled with the thermal fields evaluated according to the previous paragraph. The mechanical analysis (eq. 7-8) is run coupled with the thermal analysis (eq.1) during the cooling stage by assuming as boundary condition the temperature distribution at the end of dwell stage at 120°C.
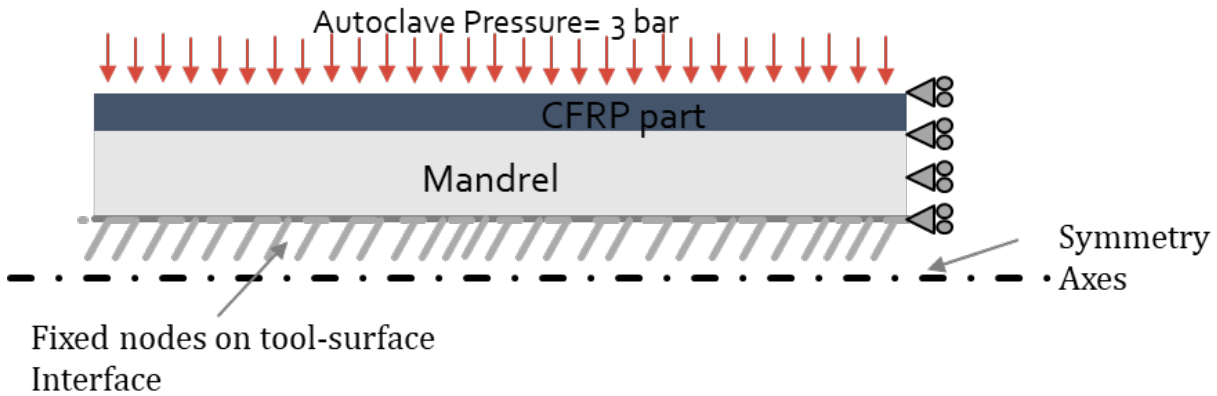
Figure 3. Mechanical boundary conditions

Results and Discussion

The standard cure cycle consists of a warmup to 120°C at 1.5 °C/min and a dwell time of 120 minutes, Figure 4 shows the temperature profile predicted by the model. Epoxy exothermic reaction results in temperature overshoots; the analysis of three different sections th=0, th=7.5 and th=15, namely the mandrel CFRP interface, the middle section and the external surface, shows temperature higher than the autoclave ambient profile. In addition, there is a temperature gradient within the cylinder, inside the CFRP part (between outer and inner radius) a difference of 20°C has been evaluated, with an average overshoot of 30°C with respect to the nominal temperature.

Overshooting is the typical behaviour of thick thermoset composite cylinders since high thickness slows down heat dissipation due to the low thermal conductivity of the composite [19]. Even if the temperature reaches a uniform distribution after 30 minutes, a dwell time of 120 min is needed to achieve the complete conversion all over the cylinder (Figure 4a). Figure 4a shows the trend of the DoC (α) vs the thermal cycle. At the end of the curing cycle, the resin reaches a value of $\alpha = 0.95$ (vitrification state), which is conventionally indicated as the complete conversion of the material. Nonetheless, due to the different temperature distribution the inner and outer surfaces of the part show a different DoC that leads to the stresses built up. Internal stresses developed inside the part are a consequence of coupling chemistry, thermal distribution, and local stiffness.

The polymers start to transfer loads when gelation occurs. A DoC in the range of 0.5 and 0.7 identifies gelation and vitrification respectively.
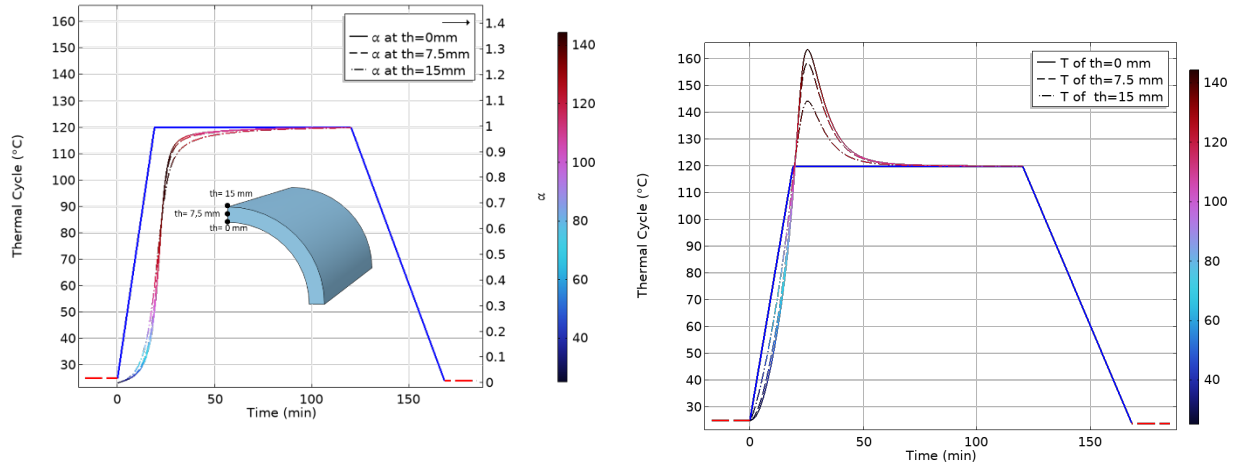
Figure 4. a) Degree of Cure (α) vs thermal cycle for point at different radii; b) Temperature profile vs thermal cycle at different radii (th=0 mm, th =7.5 mm and th= 15 mm).

As reported in Figure 4 within the part there is a variation in DoC, which leads to the formation of a differential stress field inside the part raising residual stresses at the end of the cycle.

Figure 5, reproduces the DoC map at 40 minutes, which identifies the critical situation when each point inside the part can carry loads (all the domain reached vitrification Doc>0.7) but with functionally graded properties, the maximum difference between points at different degrees of cure is:

$$\Delta = DoC_{max} - DoC_{min} \cong 0.174 \tag{12}$$
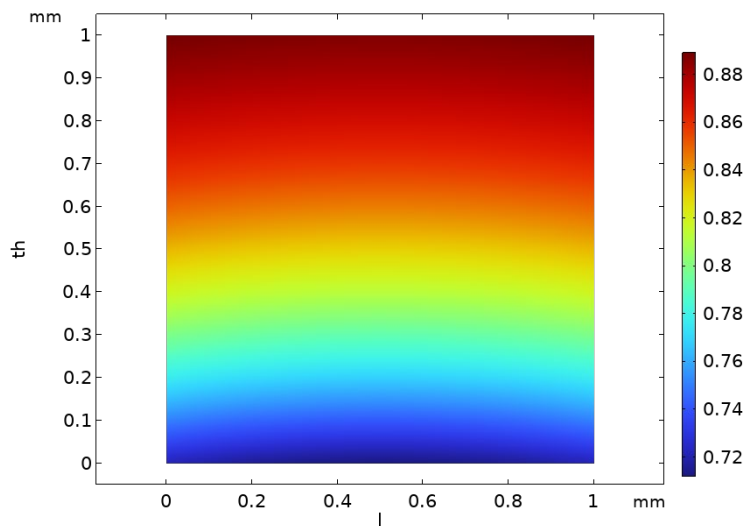
Figure 5. DoC distribution within the domain (adimensional axis) The x-axis indicates the adimensional axial length of the CFRP cylinder (l= y/250 mm), while the y-axis indicates the adimensional thickness (th = x/15 mm).

Figure 6 reproduces the stress distribution along the cooling stage, evaluated by coupling thermal and mechanical analysis. The temperature superimposed in each graph is related to the interface between mandrel and CFRP, while stresses are estimated at different sections: th=0 mm, th=7.5 mm, th=15 mm corresponding to different radius, namely th=0 is the interface between mandrel and CFRP; th=15 is the external surface of the CFRP.
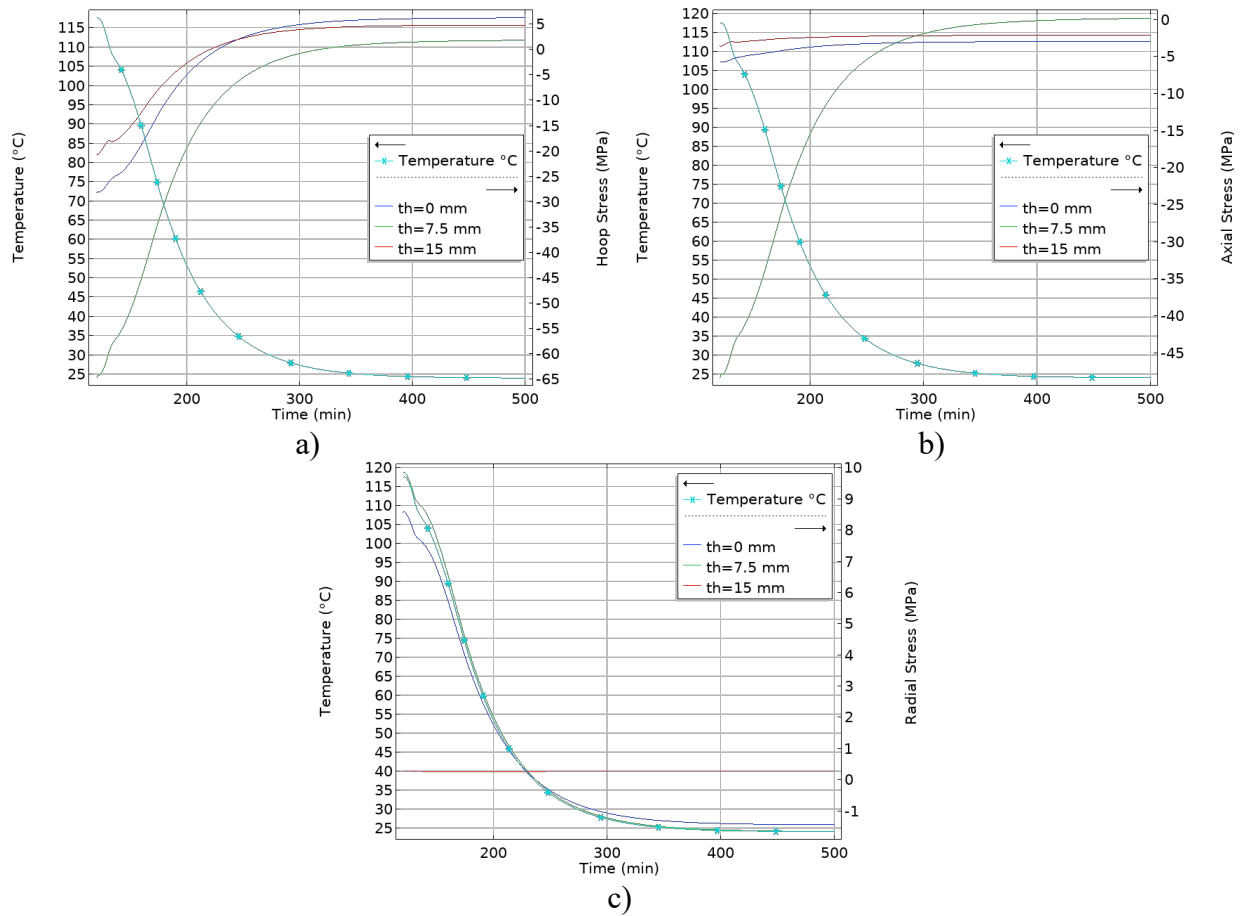
Figure 6. Stress and Temperature evolution at different radii, a) hoop, b) axial, c) radial.

The initial stress state at the precompression on the axial and tangential relaxes during the cooling stage of the axial stresses (Figure 6b).

Aiming to reduce the chance of residual stress formation, a different cure profile has been set. The rationale for defining the new profile is to minimize the degree of cure gap among the CFRP part (Δ function). A second constraint included in the optimal profile search is to minimize the temperature overshot to avoid the system reaching degradation stages.

Figure 7 depicts the DoC variation and the Temperature fields related to a double-stage cure, where a first dwell is set at 90°C for 2 hours and 30 minutes at 120°C. Numerical predictions indicate a lower overshoot (15°C) in the first dwell, and all over the cylinder, the maximum temperature reached is below the nominal cure temperature of the material (120°C).

a)   b)
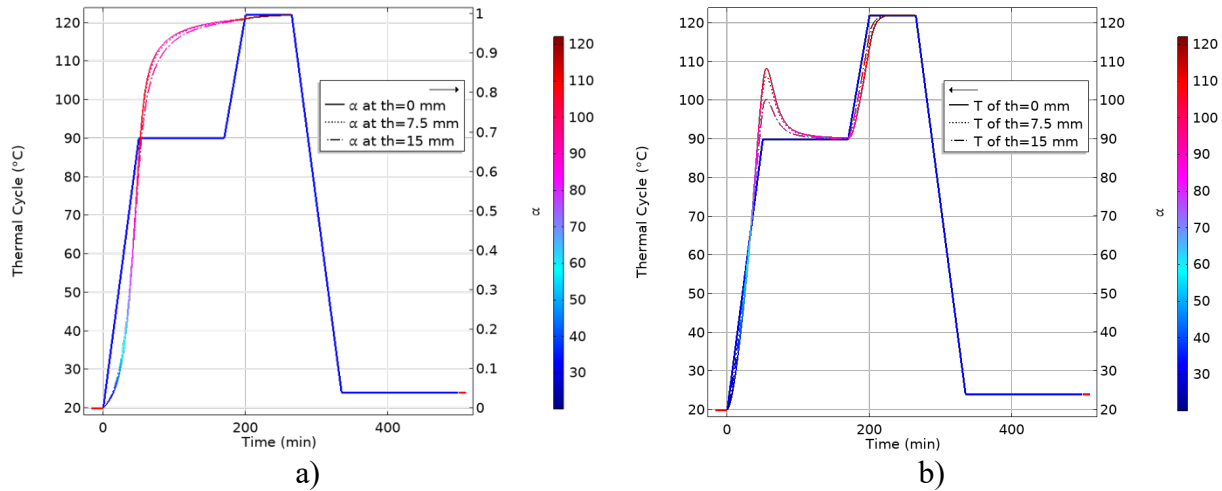
Figure 7. a) Degree of cure (α) and (b) Temperature profile vs thermal cycle optimized at different radii of the CFRP part (th=0 mm, th= 7.5 mm and th= 15 mm)

In addition, the DoC gradient inside the material is negligible, resulting in a reduction of properties mismatching (Figure 8).
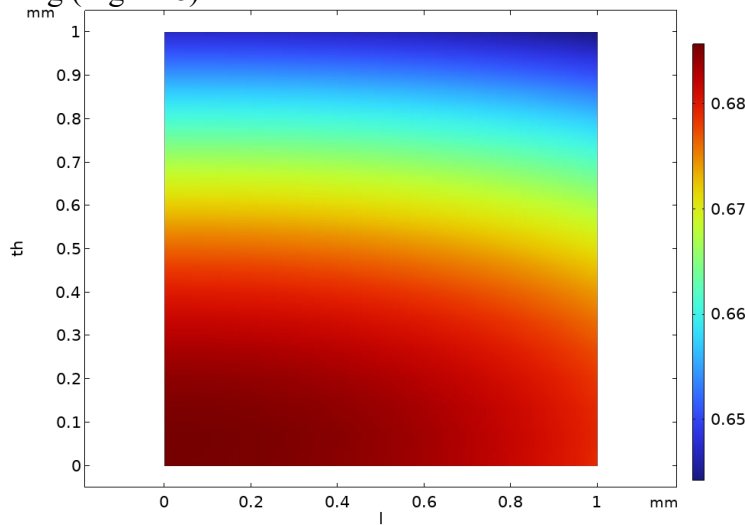
Figure 8. DoC distribution within the domain (adimensional axis). The x-axis indicates the adimensional axial length of the CFRP cylinder (l= y/250 mm), while the y-axis indicates the adimensional thickness (th = x/15 mm).

The comparison between stress distribution related to the standard cure cycle and the optional one led to a reduction in hoop stresses. The two step cure led to a smooth stresses gradient during the cure since a homogenous state of cure is achieved during the cycle. The hoop stress at the end of the cycle results in a precompression in the winding direction which should be balanced by prestressing the fiber during manufacturing. The study of axial stresses related to the standard cycle shows a risk of delamination since the maximum stresses are achieved inside the CFRP cylinder (shear stresses in the plan z, theta).
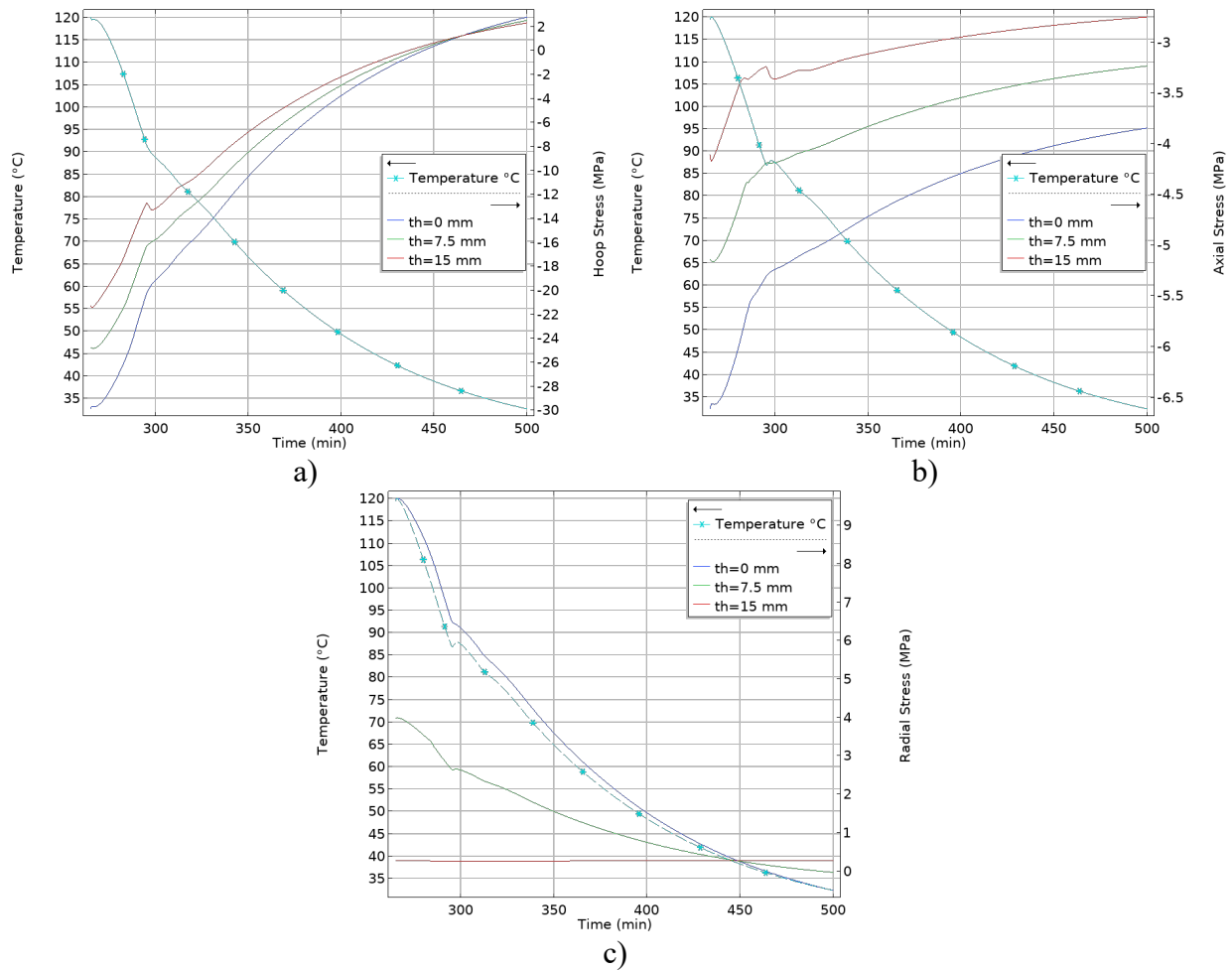
Figure 9. Stress and Temperature evolution at different radii, a) hoop, b) axial, c) radial.

The new cycle implies a reduction of interlaminar stresses, and an increase of compression is predicted at the interface between CFRP and mandrel. The latter phenomenon could depend on the boundary conditions and additional work should be addressed for overcoming the no-slip condition at the interface.

Conclusion

During thermo-set composites manufacturing, highly exothermic polymerization reaction and low heat dissipation rate due to material, lead to the development of thermal and residual stresses, especially in thick laminates, where non-uniform cure degree due to thermal gradients may also reduce material final effectiveness. In the present work, a numerical model to analyze the autoclave composite cylinder manufacturing process was developed and embedded in multiphysics software. Based on the Finite Element Method (FEM), the model considers temperature and cure dependent viscoelastic anisotropic behaviour of composite material and tool–composite interaction. Heat transfer analysis based on cure kinetics of the employed matrix was performed to assign thermal load for structural simulations. Experimental characterization of the thermal properties of the employed matrix was carried out by performing typical DSC tests.

In this paper, a multistep analysis, for predicting stress formation during the cure cycle of thick composite cylinders, was carried out. The thermal analysis was set to include the cure kinetics of the epoxy and to study the cure evolution within the domain. Subsequent analysis is executed by accounting for the thermomechanical properties during the cooling stage accounting for final stresses.

An optimal cure cycle has been identified by minimizing the Δ function which represents the maximum DoC difference within the domain. The optimal cycle led to a reduction in temperature overshoot and dramatically reduced the risk of delamination inside the CFRP cylinder.

Acknowledgement

Reference

[1] Liu, C.; Shi, Y. Design optimization for filament wound cylindrical composite internal pressure vessels considering process-induced residual stresses. *Compos. Struct.* **2020**, *235*, 111755. https://doi.org/10.1016/j.compstruct.2019.111755

[2] Kim, S.J.; Hayat, K.; Nasir, S.U.; Ha, S.K. Design and fabrication of hybrid composite hubs for a multi-rim flywheel energy storage system. *Compos. Struct.* **2014**, *107*, 19–29. https://doi.org/10.1016/j.compstruct.2013.07.032

[3] Yin, D.; Li, B.; Xiao, H. Analysis for the residual prestress of composite barrel for railgun with tension winding. *Def. Technol.* **2020**, *16*, 893–899. https://doi.org/10.1016/j.dt.2019.11.008

[4] Chen, X.; Li, Y.; Huan, D.; Wang, W.; Jiao, Y. Influence of resin curing cycle on the deformation of filament wound composites by in situ strain monitoring. *High Perform. Polym.* **2021**, *33*, 1141–1152. https://doi.org/10.1177/09540083211026359

[5] Hisada, S.; Minakuchi, S.; Takeda, N. Cure-induced strain and failure in deltoid of composite T-joints. *Compos. Part A Appl. Sci. Manuf.* **2021**, *141*, 106210. https://doi.org/10.1016/j.compositesa.2020.106210

[6] Benavente, M.; Marcin, L.; Courtois, A.; Lévesque, M.; Ruiz, E. Numerical analysis of viscoelastic process-induced residual distortions during manufacturing and post-curing. *Compos. Part A Appl. Sci. Manuf.* **2018**, *107*, 205–216. https://doi.org/10.1016/j.compositesa.2018.01.005

[7] Shokrieh, M.M.; Akbari, S.; Daneshvar, A. A comparison between the slitting method and the classical lamination theory in determination of macro-residual stresses in laminated composites. *Compos. Struct.* **2013**, *96*, 708–715. https://doi.org/10.1016/j.compstruct.2012.10.001

[8] Sorrentino, L.; Esposito, L.; Bellini, C. A new methodology to evaluate the influence of curing overheating on the mechanical properties of thick FRP laminates. *Compos. Part B Eng.* **2017**, *109*, 187–196. https://doi.org/10.1016/j.compositesb.2016.10.064

[9] He, H.-W.; Li, K.-X. Effect of Processing Parameters on the Interlaminar Shear Strength of Carbon Fiber/Epoxy Composites. *J. Macromol. Sci. Part B* **2014**, *53*, 1050–1058. https://doi.org/10.1080/00222348.2014.882249

[10] Abou Msallem, Y.; Jacquemin, F.; Boyard, N.; Poitou, A.; Delaunay, D.; Chatel, S. Material characterization and residual stresses simulation during the manufacturing process of epoxy matrix composites. *Compos. Part A Appl. Sci. Manuf.* **2010**, *41*, 108–115. https://doi.org/10.1016/j.compositesa.2009.09.025

[11] Zhang, M.; Zhang, S.; Xie, H.; Li, S. Micromechanical Analysis and Experimental Studies of Thermal Residual Stress Forming Mechanism in FRP Composites. *Appl. Compos. Mater.* **2021**, *28*, 1945–1957. https://doi.org/10.1007/s10443-021-09943-6

[12] Hu, H.; Cao, D.; Pavier, M.; Zhong, Y.; Zu, L.; Liu, L.; Li, S. Investigation of non-uniform gelation effects on residual stresses of thick laminates based on tailed FBG sensor. *Compos. Struct.* **2018**, *202*, 1361–1372. https://doi.org/10.1016/j.compstruct.2018.06.074

[13] Palmieri, B.; Petriccione, A.; De Tommaso, G.; Giordano, M.; Martone, A. An efficient thermal cure profile for thick parts made by reactive processing of acrylic thermoplastic composites. *J. Compos. Sci.* **2021**, *5*. https://doi.org/10.3390/jcs5090229

[14] Kamal, M.R.; Sourour, S. Kinetics and thermal characterization of thermoset cure. *Polym. Eng. Sci.* **1973**, *13*, 59–64. https://doi.org/10.1002/pen.760130110

[15] Patnaik, A.; Abdula; hyarani Biswas; Satapathy, A. Thermal conductivity of particulate filled polymer composites.; 2009.

[16] Macias, J.D.; Bante-Guerra, J.; Cervantes-Alvarez, F.; Rodrìguez-Gattorno, G.; Arés-Muzio, O.; Romero-Paredes, H.; Arancibia-Bulnes, C.A.; Ramos-Sánchez, V.; Villafán-Vidales, H.I.; Ordonez-Miranda, J.; et al. Thermal Characterization of Carbon Fiber-Reinforced Carbon Composites. *Appl. Compos. Mater.* **2019**, *26*, 321–337. https://doi.org/10.1007/s10443-018-9694-0

[17] Antonucci, V.; Giordano, M.; Inserraimparato, S.; Nicolais, L. Analysis of heat transfer in autoclave technology. *Polym. Compos.* **2001**, *22*, 613–620. https://doi.org/10.1002/pc.10564

[18] N. Slesinger, T. Shimizu, A. Arafath, A.P. HEAT TRANSFER COEFFICIENT DISTRIBUTION INSIDE AN AUTOCLAVE.

[19] Zhou, Y.; Li, M.; Cheng, Q.; Wang, S.; Gu, Y.; Chen, X. Quantitative relations between curing processes and local properties within thick composites based on simulation and machine learning. *Mater. Des.* **2023**, *226*, 111686. https://doi.org/10.1016/j.matdes.2023.111686